

# Use of remote sensing-derived variables in developing a forest fire danger forecasting system

Ehsan H. Chowdhury · Quazi K. Hassan

Received: 2 November 2012 / Accepted: 15 January 2013 / Published online: 26 January 2013  
© The Author(s) 2013. This article is published with open access at Springerlink.com

**Abstract** Our aim was to develop a remote sensing-based forest fire danger forecasting system (FFDFS) and its implementation in forecasting 2011 fire season in the Canadian province of Alberta. The FFDFS used Moderate Resolution Imaging Spectroradiometer (MODIS)-derived 8-day composites of surface temperature, normalized multiband drought index, and normalized difference vegetation index as input variables. In order to eliminate the data gaps in the input variables, we propose a gap-filling technique by considering both of the spatial and temporal dimensions. These input variables were calculated during the  $i$  period and then integrated to forecast the fire danger conditions into four categories (i.e., very high, high, moderate, and low) during the  $i + 1$  period. It was observed that 98.19 % of the fire fell under “very high” to “moderate” danger classes. The performance of this system was also demonstrated its ability to forecast the worst fires occurred in Slave Lake and Fort McMurray region during mid-May 2011. For example, 100 and 94.0 % of the fire spots fell under “very high” to “high” danger categories for Slave Lake and Fort McMurray regions, respectively.

**Keywords** MODIS · Normalized difference vegetation index · Normalized multiband drought index · Surface temperature · Fire spot

## 1 Introduction

Forest fire is one of the natural hazards over many forested ecosystems across the world including boreal ones. Over the boreal forested region in the Canadian province of Alberta, the annual average fire incidences were 1,541 in numbers that caused burning of approximately 220 thousand ha during the period 2002–2011 (ASRD 2012). In particular to 2011 fire season, several catastrophic fires (i.e., Slave Lake and Fort McMurray regional fires in mid-May) were observed. The Slave Lake fires were responsible for burning

---

E. H. Chowdhury · Q. K. Hassan (✉)  
Department of Geomatics Engineering, Schulich School of Engineering, University of Calgary, 2500  
University Dr NW, Calgary, AB T2N 1N4, Canada  
e-mail: qhassan@ucalgary.ca

approximately 22,000 ha of forest with an estimated economic loss of \$700 million (FTCWRC 2012); on the other hand, 595,000 ha of muskeg and bush was burned within Fort McMurray region (Treenotic 2011). In addition, fires also influence the regional biogeochemical processes (e.g., carbon cycling), climate change, etc. (Govind et al. 2011). Damages from such extensive fires have direct impact on human lives and livelihoods and also critical to the economy. Thus, it would be worthwhile to study the fire danger conditions in order to develop appropriate fire management strategies (Vadrevu et al. 2012).

In Canada, the forest fire danger conditions are calculated on daily basis using a component of Canadian Forest Fire Danger Rating System (CFFDRS), that is, known as Fire Weather Index (FWI) (Van Wagner 1987). The FWI requires point-based measurements of several weather/climatic variables (i.e., noontime air temperature, relative humidity, and wind speed; and 24-h accumulated rainfall). Consequently, the spatial dynamics of the fire danger is calculated using geographic information system (GIS)-based interpolation techniques. However, the implementation of different interpolation techniques (e.g., inverse distance weighting, spline, kriging, etc.) may produce different map outputs using the same input datasets (Chilès and Delfiner 2012). In order to eliminate these uncertainties, remote sensing-based data have greater advantage over the point-based data as it acquires the spatial variability and able to capture information over remote areas (Leblon 2005; Wang et al. 2013). In this context, our focus would be on exploring the applicability of remote sensing-based techniques in understanding the forest fire danger conditions.

The use of remote sensing-based methods for forecasting the forest fire danger conditions is not new though limited. For example, (i) Huang et al. (2008) developed a fire potential index using Moderate Resolution Imaging Spectroradiometer (MODIS) data; (ii) Guangmeng and Mei (2004) and Oldford et al. (2003) demonstrated that the NOAA AVHRR and MODIS-derived regimes of surface temperature ( $T_s$ ) were gradually increased prior to the fire occurrence; (iii) Vidal and Devaux-Ros (1995) used Landsat TM-derived normalized difference vegetation index (NDVI: a measure of vegetation greenness) in conjunction with water deficit index (WDI: defined as the difference between surface and air temperatures); and (iv) Akther and Hassan (2011a) integrated MODIS-derived variable/indice(s) of  $T_s$ , normalized multiband drought index [NMDI: a measure of water content in the canopy; (Wang and Qu 2007; Wang et al. 2008)], and temperature-vegetation wetness index [TVWI: an indirect way of estimating soil water content (Hassan et al. 2007; Akther and Hassan 2011b)].

In this paper, we opted to develop a forest fire danger forecasting system (FFDFS) by combining MODIS-derived indices (that included 8-day composites of  $T_s$ , NMDI, and NDVI) and its implementation over the boreal forested region of Alberta during the 2011 fire season. Among the two specific objectives, the first one was to implement a data gap-filling technique in replacing the null values in the primary input variables (i.e.,  $T_s$ , NMDI, and NDVI); which happened due to several reasons (e.g., cloud contamination, missing input, data fault and pixels out of bound correction, etc.). The proposed data gap-filling technique would be on the basis of integrating both of the spatial and temporal dimensions illustrated in Kang et al. (2005) and described in Sect. 3.2 in details. The second objective was to perform a quantitative evaluation between the outcome of the FFDFS (i.e., the fire danger conditions) and actual fire occurrences.

## 2 Study area and data requirements

The northern part of the Canadian province of Alberta is considered as the study area, which lies between 52–60 °N latitude and 110–120 °W longitude. It is shown in Fig. 1 using a

MODIS-derived annual land cover composite map at 500-m spatial resolution (i.e., MCD12Q1 v.005) during 2008. The study area is found to have eleven land coverage types (that include water, grasses/cereal crops, shrubs, broadleaf crops, savanna, evergreen broadleaf forest, deciduous broadleaf forest, evergreen needleleaf forest, deciduous needleleaf forest, non-vegetated, and urban). Among these, the forest types (i.e., evergreen broadleaf forest, deciduous broadleaf forest, evergreen needleleaf forest, deciduous needleleaf forest) occupy approximately 75 % of the study area, which is considered as the region of interest for forecasting the fire danger conditions. Topographically, the study area is variable in the range 162–3,596 m above the mean sea level and having a general increasing trend from north-east to south-west. Climatically, the study area experiences relative cold (mean annual temperature varies in the range  $-3.6$  to  $1.1$  °C) and dry (i.e., mean annual precipitation varies in the range 377–535 mm) conditions (Downing and Pettapiece 2006).

In addition to the above mentioned land cover map, other remote sensing data available from NASA were used in the study. The MODIS-based data products, which were 8-day composites acquired over the 2011 fire season [i.e., April–September in the range of 89–265 Julian day of year (DOY)]. These included (i) MOD11A2 v.005 product, which provided  $T_s$  images and its associated quality control (QC) information at 1-km spatial resolution. The QC was used to quantify the amount of data gaps and/or good quality pixels; (ii) MOD09A1 v.005 product, which provided surface reflectance at 7 (seven) spectral bands and its associated quality assurance (QA) information at 500-m spatial resolution. Among the seven spectral bands, the bands centered at  $0.645$   $\mu\text{m}$  (i.e., red),  $0.86$   $\mu\text{m}$  (i.e., near infrared (NIR)),  $1.64$   $\mu\text{m}$  (i.e., shortwave infrared (SWIR)), and  $2.13$   $\mu\text{m}$  (i.e., SWIR) were used. These surface reflectance images were used to calculate both NDVI and NMDI. Additionally, the QAs were used to quantify the amount of data gaps and/or good quality pixels in the NDVI and NMDI images; and (iii) MOD14A2 v.005 product, which provided fire spot images at 1-km spatial resolution. These images were used for validating the outcomes of the FFDFS.

### 3 Methodology

A schematic diagram illustrating the methods employed in this study is shown in Fig. 2. It consisted of three major components, such as (i) generating of the required input variables of the FFDFS, (ii) developing of the gap-filling algorithm and its validation, and (iii) calculating the fire danger conditions and its validation. Their brief descriptions can be found in the following subsections.

#### 3.1 Generating the required input variables of the FFDFS

##### 3.1.1 Normalized difference vegetation index (NDVI)

The NDVI is the most widely used index in the history of remote sensing. Its 8-day composite values at 500-m resolution were computed using the expression first described in (Rouse et al. 1973) as follows:

$$\text{NDVI} = \frac{\rho_{0.86} - \rho_{0.645}}{\rho_{0.86} + \rho_{0.645}} \quad (1)$$

where,  $\rho$  is the surface reflectance values of the NIR (centered at  $0.86$   $\mu\text{m}$ ) and red (centered at  $0.645$   $\mu\text{m}$ ) spectral bands.

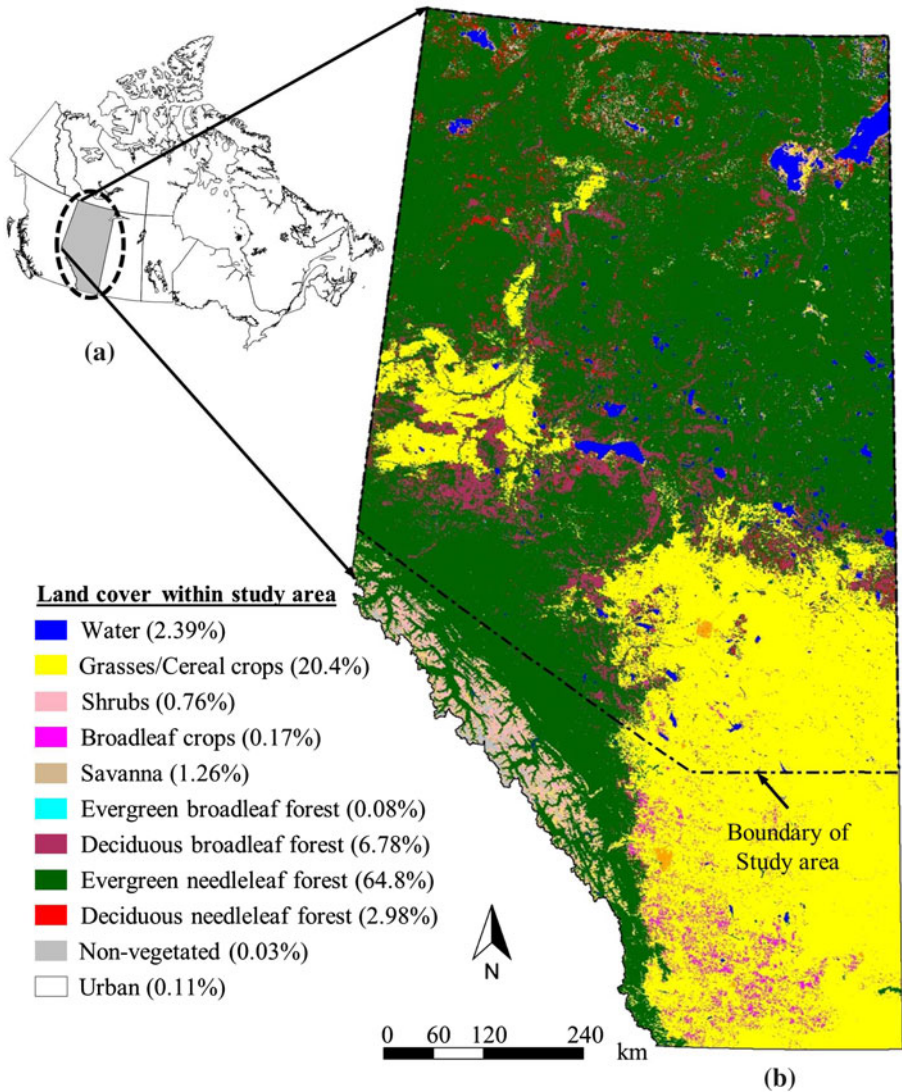


**Fig. 1** a Location of Alberta province in Canada and b extent of study area within a MODIS-derived land cover map during 2008

### 3.1.2 Normalized multiband drought index (NMDI)

The NMDI is a relatively new index first described by Wang and Qu (2007). Its 8-day composite values at 500-m resolution were computed using the following expression:

$$\text{NMDI} = \frac{\rho_{0.86} - (\rho_{1.64} - \rho_{2.13})}{\rho_{0.86} + (\rho_{1.64} - \rho_{2.13})} \quad (2)$$

where,  $\rho$  is the surface reflectance values of NIR (centered at 0.86  $\mu\text{m}$ ) and SWIR (centered at 1.64 and 2.13  $\mu\text{m}$ ) spectral bands.

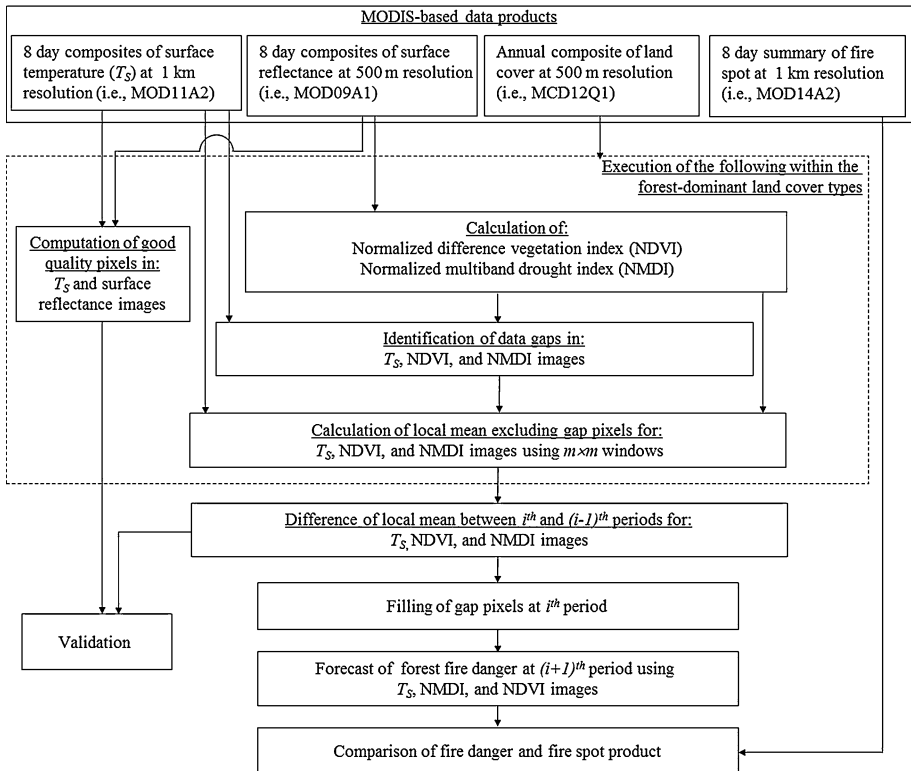


**Fig. 2** Schematic diagram of the methods employed in this study describing the proposed gap-filling algorithm and its application in forecasting forest fire danger conditions

### 3.2 Developing the gap-filling algorithm and its validation

In order to quantify the amount of data gaps in  $T_s$ , NMDI, and NDVI images; we calculated the total number of variable-specific pixels where these were not produced due to cloud effects and other reasons by considering: (i) QC image of the respective  $T_s$  images; and (ii) QA image considering both of the MODLAND QA bits and band-specific quality bits of the respective surface reflectance images for calculating both NMDI and NDVI variables. Then, we attempted to fill such gap pixels by considering both of the spatial and temporal dimensions. In the boreal landscape, the spatial extent might vary gradually within similar land cover types and temporal dimension might influence significant changes in temperature, greenness and moisture conditions within the 8-day time period. Our proposed gap-filling algorithm was as follows:

$$X(i) = X(i - 1) \pm Abs\{\bar{X}(i)_{m \times m} - \bar{X}(i - 1)_{m \times m}\} \tag{3}$$

where,  $X(i)$  and  $X(i - 1)$  are the infilled and non-gap values for the variables (i.e.,  $T_s$ /NMDI/NDVI) of interest during  $i$  and  $i - 1$  period, respectively;  $\bar{X}(i)_{m \times m}$  and  $\bar{X}(i - 1)_{m \times m}$  are the mean values of the variables (i.e.,  $T_s$ /NMDI/NDVI) of interest for the window size of  $m \times m$  during  $i$  and  $i - 1$  period, respectively. The mean values of the variables were computed based on different moving window sizes (i.e., in the range  $3 \times 3$ –

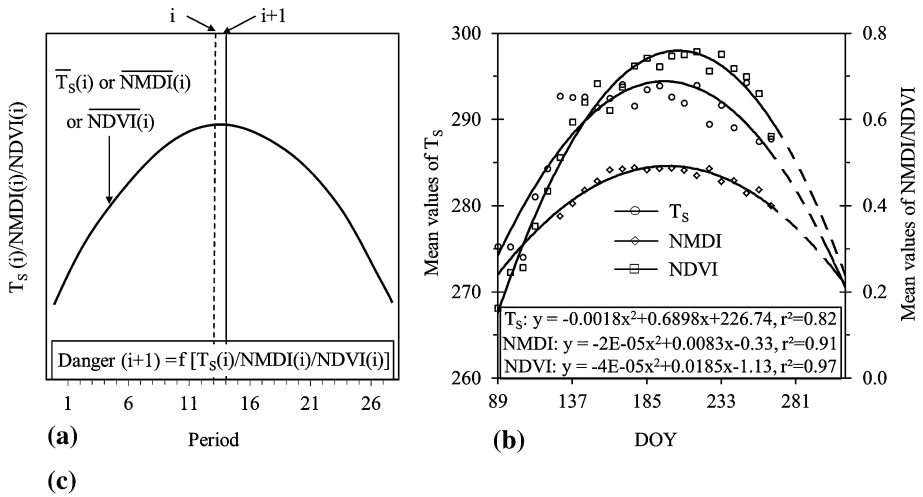
$15 \times 15$ ) within the selected land cover types. So, thus, we obtained mean value images for each 8-day period according to different window sizes. The absolute deviation of the mean values of the variables during  $i$  and  $i - 1$  period for  $m \times m$  window size was added with the instantaneous value at  $i - 1$  period when the mean value at  $i$  period was found to be larger than  $i - 1$  period. Similarly, the absolute deviation of the mean values was subtracted from the instantaneous value at  $i - 1$  period when the mean value at  $i$  period was found to be smaller than  $i - 1$  period. The process would initiate with the smallest window size (i.e.,  $3 \times 3$ ) and then check whether the filling would complete by recalculating the remaining gap pixels in the image. If not, the remaining gap pixels would be filled by increasing the window size to next level (i.e., in the range  $5 \times 5$  to  $15 \times 15$ ). Note that the increment of the window would depend on the status of filling condition and only be performed on the remaining gap pixels. In some instances, the employment of even  $15 \times 15$  window size might be unable to fill the gaps. Then, we might consider the window size equivalent to the entire study area of selected land covers. In the implementation of the above gap-filling algorithm, it was assumed that the probability of a particular pixel having data gap within 16 days would be very rare. In such cases, filling data gap at  $i$  period would not be possible if gap-free pixels at  $i - 1$  period were found to be absent.

In reality, it would not be possible to verify the accuracy of the above described algorithm due to the fact that level and local occurrence of cloud formation and other causes is extremely difficult to measure. However, we performed a validation by synthetically treating good quality pixels as gap ones; and quantified statistically by determining coefficient of determination ( $r^2$ ) and root mean square error (RMSE). Note that such good pixels were retrieved based on the following criterion: (i) for  $T_S$  when the average  $T_S$  errors were found to be either equal or less than 2 K; and (ii) for surface reflectance, we employed a set of parameters, such as MOD35 cloud (i.e., clear), cloud shadow (i.e., no), aerosol quality (i.e., climatology and low), cirrus detected (i.e., none and small), internal cloud algorithm flag (i.e., no cloud), and pixel to adjacent to cloud (i.e., no).

### 3.3 Calculating the fire danger conditions and its validation

We employed 8-day composites of MODIS-derived input variables of  $T_S$ , NMDI, and NDVI in the proposed FFDFS framework (see Fig. 3a for details). The FFDFS consisted of three steps. In first step, we calculated the study area-specific mean values for the input variables during the  $i$  period [i.e.,  $\overline{T_S}(i)$ ,  $\overline{NMDI}(i)$ ,  $\overline{NDVI}(i)$ ]; and their associated seasonal dynamics are shown in Fig. 3b. In second step, we determined the individual input variable-specific danger conditions (either high or low, see Fig. 3c) during  $i + 1$  period upon comparing the instantaneous values of each of the input variables at a given pixel from  $i$  period [i.e.,  $T_S(i)$ ,  $NMDI(i)$ ,  $NDVI(i)$ ] with their respective mean values [i.e.,  $\overline{T_S}(i)$ ,  $\overline{NMDI}(i)$ ,  $\overline{NDVI}(i)$ ] calculated in first step. Finally, we combined the individual input variable-specific danger conditions determined in second step into four categories, such as (i) very high: if all the three variables demonstrated that the fire danger would be high; (ii) high: if at least two of the three variables demonstrated that the fire danger would be high; (iii) moderate: if at least one of the three variables demonstrated that the fire danger would be high; and (iv) low: if all of the three variables demonstrated that the fire danger would be low.

Upon generating the fire danger maps, we compared them with the MODIS-derived fire spot images on cell-to-cell basis in order to evaluate the performance of the FFDFS. The integration of individual input variables (e.g.,  $T_S$ , NMDI, and NDVI) of different spatial resolution was done so that the geometric element and object structure, for example,



Input variables	Danger (i+1)		Comments
	High	Low	
$T_s(i)$	$\geq \overline{T_s(i)}$	$< \overline{T_s(i)}$	High temperature favor fire
$NMDI(i)$	$\leq \overline{NMDI(i)}$	$> \overline{NMDI(i)}$	Low moisture in vegetation may support fire
$NDVI(i)$	$\leq \overline{NDVI(i)}$	$> \overline{NDVI(i)}$	Low greenness may support to initiate fire as it relates with a set of biophysical variables

**Fig. 3** a The conceptual diagram of FFDFS, b study area-specific average values for  $T_s$ , NMDI, and NDVI variables for 2011 fire season (i.e., between 89 and 265 DOY), c the criterion of describing fire danger conditions for the input variables of  $T_s$ , NMDI, and NDVI

gridded pixels of the datasets would match to each other. The data integration was done in two steps in the FFDFS, that is, (i) the  $T_s$  images were resampled at 500 m from 1 km prior to integrate with the NMDI and NDVI variables having 500-m spatial resolution; and (ii) the fire spot images were also resampled at 500-m spatial resolution prior to comparison with the fire danger condition maps having 500-m spatial resolution.

### 4 Results and discussion

#### 4.1 Evaluation of gap-filling algorithm

We found that the amount of data gaps was approximately 11.41, 0.86, and 0.08 % in the  $T_s$ , NMDI, and NDVI images, respectively, during the entire study period (Fig. 4). Relatively high amount of data gaps in the  $T_s$  images were observed due to the fact that the quality of the MODIS-based  $T_s$  products would be often contaminated to a large scale as a matter of inherent limitation of the thermal infrared remote sensors (i.e., retrieved only in clear-sky conditions) (Wan 2008).

Upon implementing the proposed gap-filling algorithm, we used five (5) imaging periods for each of the  $T_s$ , NMDI, and NDVI images for evaluating its performance, which were well distributed over the entire growing season. The use of the  $3 \times 3$  window size

revealed that approximately 84.14 and 100 % of the data gaps were filled for  $T_S$  and both NMDI and NDVI images, respectively. During the period of validation, our analyses showed strong agreements of the predicted values for the variable of interest with the observed data (i.e., the good quality pixels which were declared as data gaps). For example, the slope,  $r^2$ , and RMSE values were on an average: (i) 0.94, 0.88, and 0.883 K, respectively, for  $T_S$  images (see Fig. 5 for details); (ii) 0.93, 0.91, and 0.021, respectively,

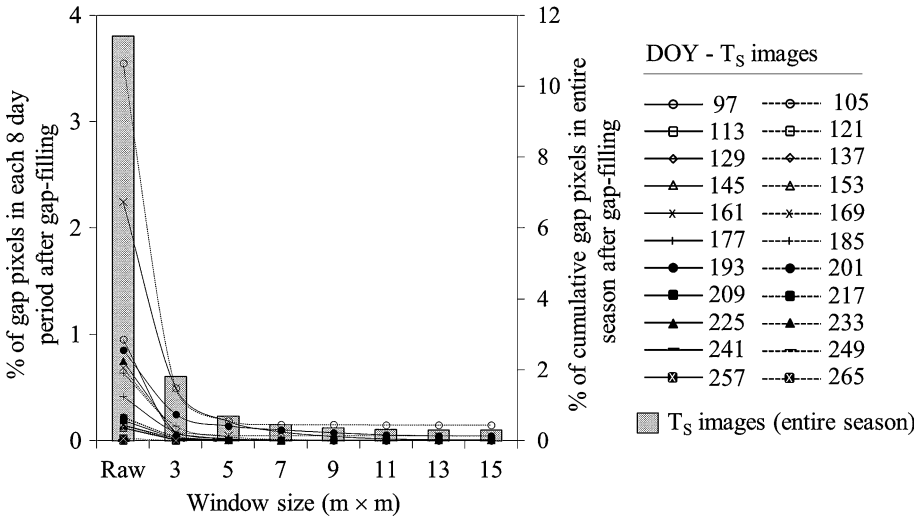


**Fig. 4** Percentage of gap pixels in  $T_S$  images upon gap-filling using various window sizes

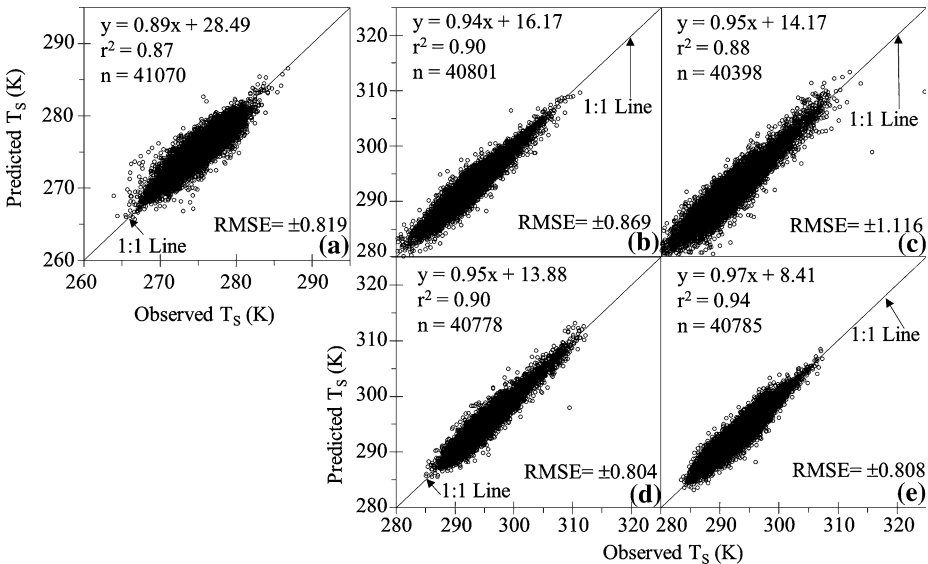


**Fig. 5** Comparison between observed and predicted  $T_S$  upon using  $3 \times 3$  window size for gap-filling: **a** 97 DOY,  $F = 286507$ ,  $p$  value  $< 0.0001$  **b** 137 DOY,  $F = 368260$ ,  $p < 0.0001$  **c** 177 DOY,  $F = 320805$ ,  $p < 0.0001$ , **d** 217 DOY,  $F = 382576$ ,  $p < 0.0001$ , **e** 249 DOY,  $F = 607077$ ,  $p < 0.0001$



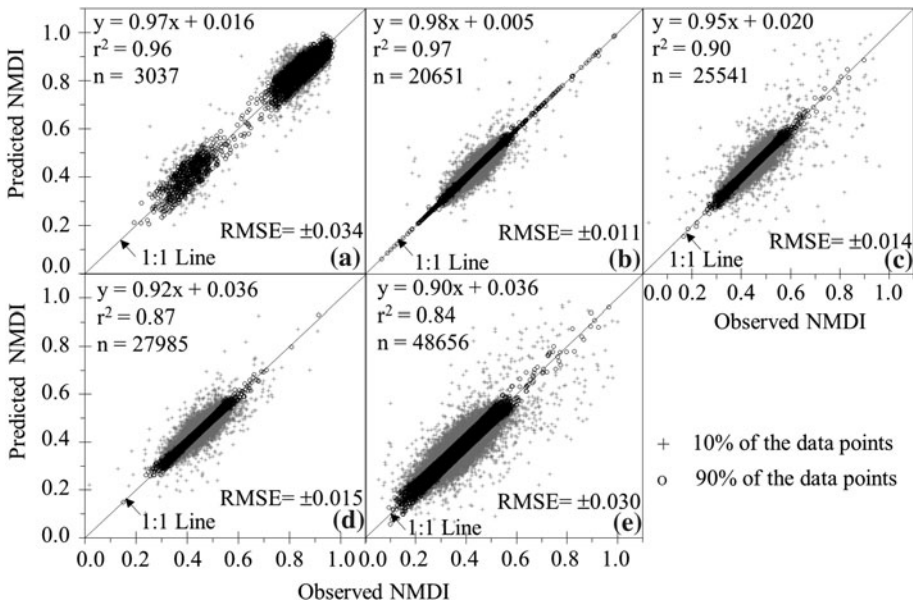


**Fig. 6** Comparison of observed and predicted NMDI upon using  $3 \times 3$  window size for gap-filling: **a** 113 DOY,  $F = 18880$ ,  $p < 0.0001$ , **b** 153 DOY,  $F = 241571$ ,  $p < 0.0001$ , **c** 193 DOY,  $F = 263602$ ,  $p < 0.0001$ , **d** 233 DOY,  $F = 111437$ ,  $p < 0.0001$ , **e** 265 DOY,  $F = 510446$ ,  $p < 0.0001$

for NMDI images for 90 % of the data points (Fig. 6); and (iii) 0.97, 0.93, and 0.021, respectively, for NDVI images for 90 % of the data points (Fig. 7). The observed RMSE values for both  $T_S$  (i.e., 0.80–1.12 K; Fig. 5) and NDVI (i.e., 0.017–0.024; Fig. 7) gap-filling were similar to other study, such as (i) MODIS-derived  $T_S$  values in comparison with ground-based such measurements over homogeneous rice fields and forested areas yielded a RMSE of 0.70 K (Coll et al. 2009); (ii) MODIS-derived NDVI values over the good quality pixels were within an error bar of  $\pm(0.02 + 2 \% \text{NDVI})$  for 97.11 % of the observations (Vermote and Kotchenova 2008); and (iii) the evaluation of MODIS-derived NDVI over all of the land cover types at Jornada Experimental Range in New Mexico, USA in comparison with MODIS Quick Airborne Looks-based observations showed RMSE values less than 0.03 (Gao et al. 2003). So far, we did not find studies reporting accuracy information associated with NMDI retrieval or gap-filling. However, we might consider that the observed RMSE values for NMDI (i.e., 0.011–0.034) would be reasonable due to their similarities with that of NDVI. It would be the case as both of the NMDI and NDVI were calculated as a function of surface reflectance.

In the case of  $T_S$  images, we required to increase the window size (in the range from  $5 \times 5$  to  $15 \times 15$ ; and also entire study area) in order to gap-filling the remaining data gaps (i.e.,  $\sim 15.86 \%$ ). For each of the window size, we compared the predicted values with the observed data (i.e., the good quality pixels which were declared as data gaps); and calculated RMSE and  $r^2$  values (see Table 1 for details). It revealed that both of the RMSE and  $r^2$  values were deteriorating with the increment of the window sizes (e.g.,  $\text{RMSE} \approx 1.097 \text{ K}$  and  $r^2 \approx 0.85$  for  $5 \times 5$  window size;  $\text{RMSE} \approx 1.444 \text{ K}$  and  $r^2 \approx 0.75$  for  $15 \times 15$  window size; and  $\text{RMSE} \approx 2.380 \text{ K}$  and  $r^2 \approx 0.36$  for the window size equal to the study area). These finding would be reasonable due to the fact that the spatial integrity would start to fall apart with the increment of the search window (Girard and Girard 2003; Li and Heap 2011).

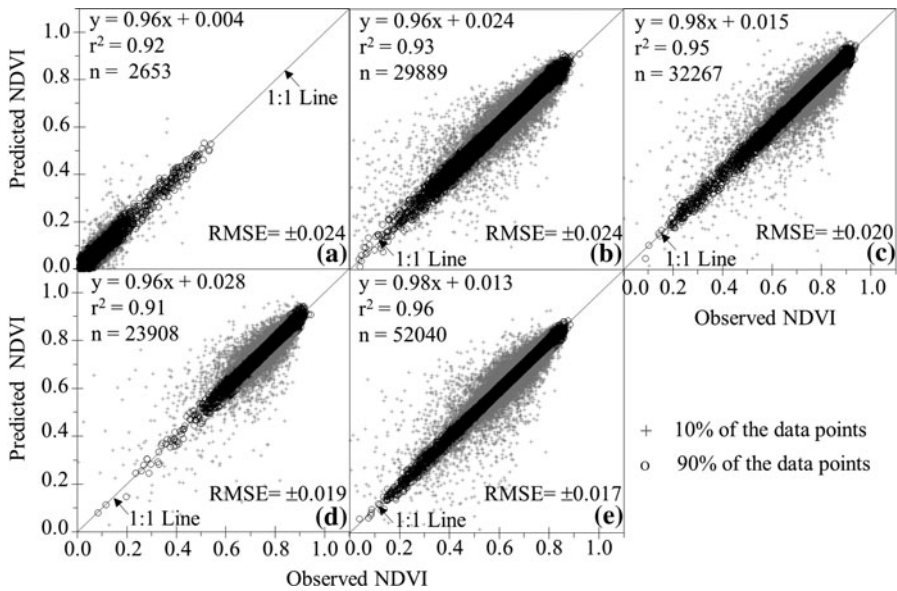


**Fig. 7** Comparison of observed and predicted NDVI upon using 3 × 3 window size for gap-filling: **a** 105 DOY,  $F = 18880$ ,  $p < 0.0001$ , **b** 145 DOY,  $F = 241571$ ,  $p < 0.0001$ , **c** 185 DOY,  $F = 263602$ ,  $p < 0.0001$ , **d** 225 DOY,  $F = 111437$ ,  $p < 0.0001$ , **e** 257 DOY,  $F = 510446$ ,  $p < 0.0001$

**Table 1** Coefficient of determination ( $r^2$ ) and root mean square error (RMSE) between observed and predicted  $T_s$  variable using different window size

Window size	DOY										Average	
	97		137		177		217		249		$r^2$	RMSE
	$r^2$	RMSE	$r^2$	RMSE	$r^2$	RMSE	$r^2$	RMSE	$r^2$	RMSE		
3 × 3	0.87	0.819	0.90	0.869	0.89	1.116	0.90	0.804	0.94	0.808	0.90	0.883
5 × 5	0.81	1.009	0.85	1.085	0.83	1.413	0.86	0.994	0.91	0.981	0.85	1.096
7 × 7	0.77	1.112	0.81	1.215	0.79	1.583	0.82	1.106	0.89	1.085	0.81	1.220
9 × 9	0.74	1.178	0.79	1.305	0.76	1.693	0.80	1.181	0.87	1.150	0.79	1.301
11 × 11	0.72	1.227	0.76	1.371	0.74	1.768	0.78	1.234	0.86	1.210	0.77	1.362
13 × 13	0.70	1.264	0.75	1.424	0.73	1.824	0.77	1.274	0.85	1.235	0.76	1.404
15 × 15	0.69	1.295	0.73	1.468	0.71	1.868	0.76	1.306	0.85	1.285	0.75	1.444
Study area	0.20	2.116	0.42	2.328	0.49	2.626	0.33	2.233	0.37	2.597	0.36	2.380

Also, it would be worthwhile to note that both of the window size (i.e., 15 × 15 and the study area) were not able to gap-filling similar portion of the data gaps (i.e., ~0.295 % of the data gaps; see Fig. 4). Under these circumstances, we considered that the choice of 15 × 15 window size would be appropriate because it produced reasonable agreements (i.e.,  $RMSE \approx 1.444$  K and  $r^2 \approx 0.75$ ) in comparison with that of the window size equal to the entire study area (i.e.,  $RMSE \approx 2.380$  K and  $r^2 \approx 0.36$ ). The rationale behind the inability to gap-filling all of the data gaps would be due to the absence of gap-free pixels in both temporal and spatial dimensions (Kang et al. 2005).

### 4.2 Evaluation of the FFDFS

During study period, the temporal dynamics of study area-specific average values of the  $T_S$ , NMDI, and NDVI variables showed distinct patterns (Fig. 3b), which were identical to the generalized ones shown in Fig. 3a. Upon applying quadratic fits to the variable of interest as a function of DOY, we found strong relations having  $r^2$  values of 0.82, 0.91, and 0.97 for  $T_S$ , NMDI, and NDVI, respectively.

Table 2 shows the outcomes of the FFDFS using the combinations of input variables (i.e.,  $T_S$ , NMDI, and NDVI) as per the criterion illustrated in Fig. 3c. These outcomes were compared with the % of pixels represented by the fire spots. The combined variables revealed strong agreements, where 98.19 % of fire fell under the categories from “very high” to “moderate” danger classes, respectively. However, the small amount of disagreements (i.e., 1.81 %) between the predictions and fire spots could be attributed by other factors, such as precipitation, wind speed, topography, fuel cover types, phenological variability (Leblon et al. 2001; Oldford et al. 2003; Desbois and Vidal 1996; Ardakani et al. 2011; De Angelis et al. 2012), which were beyond the scope of this study. It would be interesting to note that similar results were demonstrated by Akther and Hassan (2011a). For example, the combination of  $T_S$ , NMDI, and TVWI variables revealed 91.6 % of the fires spots fell under “very high” to “moderate” danger classes when compared between the fire danger categories and actual fire occurrences data during the period of 2006–2008 fire seasons. Despite the similar results, our study addressed two major drawbacks of Akther and Hassan (2011a); such as the implementation of a data gap-filling technique for the pixels having null values and the replacement of TVWI using NDVI. Such replacement would be critical as the computation of TVWI was complex, due to the interpretation of the scatter plots of  $T_S$  and NDVI requires extensive knowledge and potentially differs from person to person.

During the second week of May 2011, the study area experienced several severe fires. Thus, we opted to evaluate the performance of the FFDFS during the period May 9–16, 2011, which were calculated as a function of the combined input variables of  $T_S$ , NMDI and NDVI acquired during the prior period (i.e., May 1–8, 2011) (see Fig. 8 for details). The fire danger map revealed that ~ 17.4, 34.1, and 35.6 % of the pixels fell under danger categories of “very high,” “high,” and “moderate” for the entire study area. In addition, fire danger conditions were analyzed further over both of Slave Lake and Fort McMurray regions (where the worst fires were occurred during the recent history) (see Fig. 8b). It revealed that 100 and 94 % of the fire spots fell under “very high” to “high” danger classes for Slave Lake and Fort McMurray regions, respectively. Thus, the effectiveness of the FFDFS in forecasting devastating fires was also proved.

In this paper, the input variables of the FFDFS were derived using different spectral bands of MODIS products which might not be autocorrelated. Because the  $T_S$  was derived

**Table 2** Percentage of data under each fire danger categories using combined input variables of  $T_S$ , NMDI, and NDVI in comparison with the fire spot

Combination of input variables	No. of input variables satisfying the fire danger conditions	Fire danger classes	% of data	Cumulative % of data
$T_S$ , NMDI, and NDVI	All	Very high	49.13	49.13
	At least 2	High	38.91	88.04
	At least 1	Moderate	10.15	98.19
	None	Low	1.81	100.00

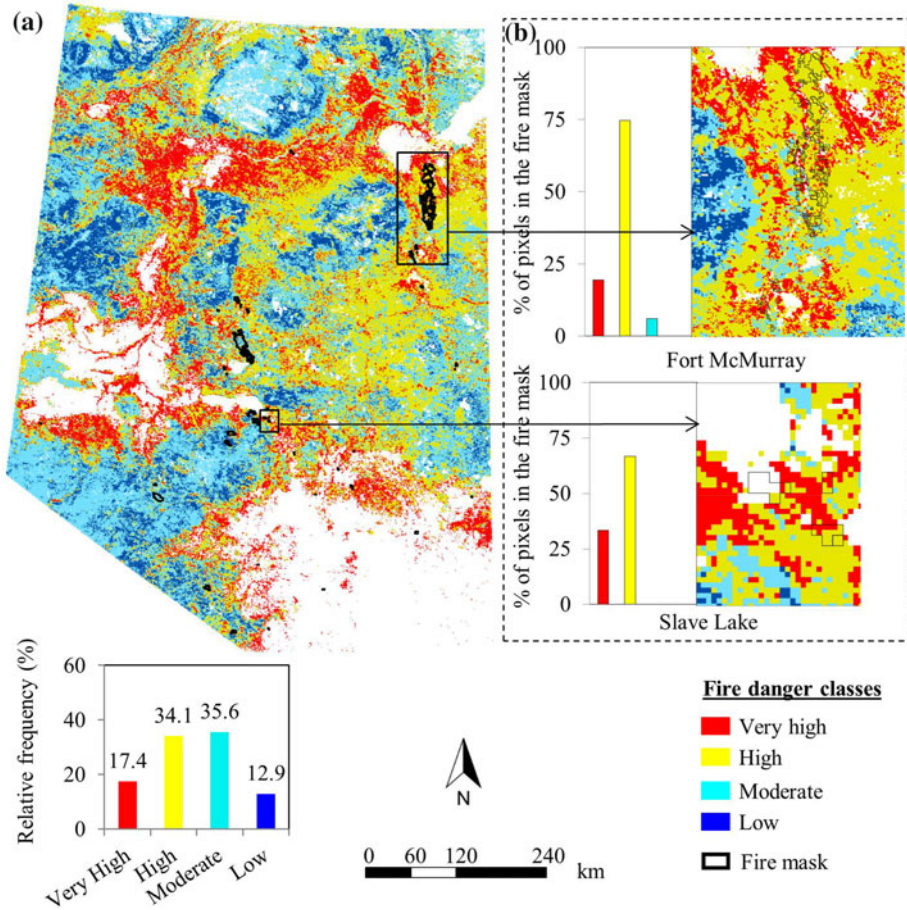


**Fig. 8** Example Fire danger map for the period May 9–16, 2011, generated by combining the  $T_s$ , NMDI, and NDVI variables acquired during the prior 8-day period (i.e., May 1–8, 2011)

from the thermal bands in between 10.78 and 12.27  $\mu\text{m}$ ; NMDI was computed based on the spectral bands centered at 0.86  $\mu\text{m}$  (controls cell structure of the plant leaves), 1.64, and 2.13  $\mu\text{m}$  (controls water content of the leaves); and NDVI was derived from spectral bands centered at 0.645  $\mu\text{m}$  (chlorophyll absorption band) and 0.86  $\mu\text{m}$ , respectively. Though the NIR band (i.e., 0.86  $\mu\text{m}$ ) was used in calculating both the NDVI and NMDI variables along with other spectral bands (see Eqs 2 and 3); thus, we might assume no autocorrelation between them. The validation of the FDFFS was also done using the fire spot data as a function of 3.9  $\mu\text{m}$  (fire detection and characterization) and 11  $\mu\text{m}$  (fire detection and cloud masking) thermal bands during the  $i + 1$  period, while the input variables were calculated during  $i$  period. Thus, it could be considered not be autocorrelated despite that MODIS data were used in both formulation and validation of the FDFFS.

## 5 Conclusions

In this paper, we proposed a simple protocol in order to filling the data gaps in the 8-day composites of MODIS-derived  $T_s$ , NMDI, and NDVI on the basis of both spatial and

temporal connotations. It revealed that the use of the  $3 \times 3$  window size would infill approximately 84.14 and 100 % of the data gaps for  $T_S$  and both NMDI and NDVI images, respectively. In these cases, we also observed strong agreements between the predicted values for the variable of interest with the observed data (i.e., the good quality pixels which were declared as data gaps), such as  $r^2$ , and RMSE values were on an average: (i) 0.88 and 0.883 K, respectively, for  $T_S$  images; (ii) 0.91 and 0.021, respectively, for NMDI images; and (iii) 0.93 and 0.021, respectively, for NDVI images. In order to filling the remaining data gaps (i.e.,  $\sim 15.86$  %) for  $T_S$  images, we increased window size (in the range from  $5 \times 5$  to  $15 \times 15$ ); and both of the RMSE and  $r^2$  values were still found to be in the reasonable bounds (i.e., RMSE  $\approx 1.096$  K and  $r^2 \approx 0.85$  for  $5 \times 5$  window size; RMSE  $\approx 1.444$  K and  $r^2 \approx 0.75$  for  $15 \times 15$  window size). In addition, the combination of  $T_S$ , NMDI, and NDVI also produced good results (i.e., 98.19 % of the fire fell under “very high” to “moderate” danger classes). Thus, the proposed methods would be an effective operational framework of FPDFS.

**Acknowledgments** The study was funded by a NSERC Discovery Grant to Dr. Hassan. We are indebted to NASA for providing the MODIS data at free of cost. In addition, we would like to acknowledge the anonymous reviewers for commenting on our paper.

**Open Access** This article is distributed under the terms of the Creative Commons Attribution License which permits any use, distribution, and reproduction in any medium, provided the original author(s) and the source are credited.

## References

- Akther MS, Hassan QK (2011a) Remote sensing based assessment of fire danger conditions over boreal forest. *IEEE J Sel Top Appl Earth Obs Remote Sens* 4:992–999
- Akther MS, Hassan QK (2011b) Remote sensing based estimates of surface wetness conditions and growing degree days over northern Alberta, Canada. *Boreal Environ Res* 16:407–416
- Ardakani AS, Zoej MJV, Mohammadzadeh A, Mansourian A (2011) Spatial and temporal analysis of fires detected by MODIS data in northern Iran from 2001 to 2008. *IEEE J Sel Topics Appl Earth Obs Remote Sens* 4(1):216–225
- ASRD (Alberta Sustainable Resource Development) (2012) 10-Year Wildfire Statistics. <http://www.srd.alberta.ca/Wildfire/WildfireStatus/HistoricalWildfireInformation/10-YearStatisticalSummary.aspx> (Last visited 25 June, 2012)
- Chilès J-P, Delfiner P (2012) Geostatistical modeling spatial uncertainty, 2nd edn. Wiley, Hoboken 699p
- Coll C, Wan Z, Galve JM (2009) Temperature-based and radiance-based validations of the V5 MODIS land surface temperature product. *J Geophys Res* 114:D20102. doi:10.1029/2009JD012038
- De Angelis A, Bajocco S, Ricotta C (2012) Phenological variability drives the distribution of wildfires in Sardinia. *Landsc Ecol*. doi:10.1007/s10980-012-9808-2
- Desbois N, Vidal A (1996) Real time monitoring of vegetation flammability using NOAA-AVHRR thermal infrared data. *EARSEL Adv Remote Sens* 4(4-XI):25–32
- Downing DJ, Pettapiece WW (2006) Natural Regions and Subregions of Alberta. Pub. No. T/852. Natural Regions Committee: Government of Alberta, Alberta, Canada, [http://tpr.alberta.ca/parks/heritageinfo/centre/docs/NRSRcomplete%20May\\_06.pdf](http://tpr.alberta.ca/parks/heritageinfo/centre/docs/NRSRcomplete%20May_06.pdf) (Last visited 10 April, 2012)
- FTCWRC (Flat Top Complex Wildfire Review Committee) (2012) Flat top complex. Submitted to the Minister of Alberta Environment and Sustainable Resource Development. <http://www.srd.alberta.ca/Wildfire/WildfirePreventionEnforcement/WildfireReviews/documents/FlatTopComplex-WildfireReviewCommittee-May18-2012.pdf> (Last visited 25 June, 2012)
- Gao X, Huete AR, Didan K (2003) Multi sensor comparisons and validation of MODIS vegetation indices at the semiarid Jornada experimental range. *IEEE Trans Geosci Remote Sens* 41(10):2368–2381
- Girard M-C, Girard CM (2003) Processing of remote sensing data. A.A. Balkema, India 291p
- Govind A, Chen JM, Bernier P, Margolis H, Guindon L, Beaudoin A (2011) Spatially distributed modeling of the long-term carbon balance of a boreal landscape. *Ecol Model* 222(2011):2780–2795

- Guangmeng G, Mei Z (2004) Using MODIS land surface temperature to evaluate forest fire risk of northeast China. *IEEE Geosci Remote Sens Lett* 1(2):98–100
- Hassan QK, Bourque CPA, Meng FR, Cox RM (2007) A wetness index using terrain corrected surface temperature and NDVI derived from standard MODIS products: an evaluation of its use in a humid forest dominated region of eastern Canada. *Sensors* 7:2028–2048
- Huang B-h, Titan L, Zhou L-x, Shi C-q (2008) The fire potential index (FPI) based on MODIS data and its application. *Remote Sens Land Resour* 20(3):56–60
- Kang S, Running WS, Zhao M, Kimball SJ, Glassy J (2005) Improving continuity of MODIS terrestrial photosynthesis products using an interpolation scheme for cloudy pixels. *Int J Remote Sens* 26:1659–1679
- Leblon B (2005) Using remote sensing for fire danger monitoring. *Nat Hazards* 35:343–359
- Leblon B, Alexander M, Chen J, White S (2001) Monitoring fire danger of northern boreal forests with NOAA-AVHRR NDVI images. *Int J Remote Sens* 22(14):2839–2846
- Li J, Heap AD (2011) A review of comparative studies of spatial interpolation methods in environmental sciences: performance and impact factors. *Ecol Inform* 6:228–241
- Oldford S, Leblon B, Gallant L, Alexander ME (2003) Mapping pre-fire forest conditions with NOAA-AVHRR images in northern boreal forests. *Geocarto Int* 18(4):21–32
- Rouse JW, Hass RH, Schell JA, Deering DW (1973) Monitoring vegetation systems in the Great Plains with ERTS. NASA SP-351, Washington, DC NASA, Third ERTS-1 symposium, pp 309–317
- Treenotic Inc. (2011) Alberta firefighters fighting biggest fire they've ever fought. <http://foresttalk.com/index.php/2011/06/16/alberta-firefighters-fighting-biggest-fire-theyve-ever-fought/> (Last visited May 18, 2012)
- Vadrevu KP, Csiszar I, Ellicott E, Giglio L, Badarinath KVS, Vermote E, Justice C (2012) Hotspot analysis of vegetation fires and intensity in the Indian region. *IEEE J Sel Topics Appl Earth Obs Remote Sens*. doi:10.1109/JSTARS.2012.2210699
- Van Wagner CE (1987) Development and structure of the Canadian forest fire weather index. Government of Canada, Canadian Forestry Service, Petawawa National Forestry Inst., Ottawa, 37 p
- Vermote EF, Kotchenova S (2008) Atmospheric correction for the monitoring of land surfaces. *J Geophys Res* 113:D23S90. doi:10.1029/2007JD009662
- Vidal A, Devaux-Ros C (1995) Evaluating forest fire hazard with a Landsat TM derived water stress index. *Agric For Meteorol* 77:207–224
- Wan Z (2008) New refinements and validation of the MODIS land-surface temperature/emissivity products. *Remote Sens Environ* 112:59–74
- Wang L, Qu JJ (2007) NMDI: a normalized multi-band drought index for monitoring soil and vegetation moisture with satellite remote sensing. *Geophys Res Lett* 34:L20405
- Wang L, Qu JJ, Hao X (2008) Forest fire detection using the normalized multi-band drought index (NMDI) with satellite measurements. *Agric For Meteorol* 148:1767–1776
- Wang L, Zhou Y, Zhou W, Wang S (2013) Fire danger assessment with remote sensing: a case study in Northern China. *Nat Hazards* 65:819–834